Chapter 3

Computational fluid dynamics analyses

3.1 Introduction

In this chapter the ES 208 Tail gas heat exchanger that was selected in the previous chapter, is used in a number of Computational Fluid Dynamics (CFD) analyses. The complete heat exchanger could not be simulated, because of a limitation in computational power and therefore only small representative sections of the heat exchanger were analysed. First a repeating section of the middle part of the heat exchanger was analysed and then an equivalent porous model was obtained. The second part was to analyse the inlet section together with the porous model to obtain the necessary boundary conditions for the model. GAMBIT (1999) was used to generate and mesh the models and FLUENT (1999) was used to solve the models.

3.2 CFD analyses: Middle section of heat exchanger

Since the baffle pattern is repeated 4 times, only one of the repeating sections was used to obtain the pressure drop, flow patterns and velocities through the heat exchanger section. The heat exchanger section is symmetric about the x- and y-axes, therefore only a quarter section was simulated (see figure 3.1).

A mesh of 657 104 cells was generated in GAMBIT. This mesh was adapted and solved in FLUENT using a two-equation turbulent energy and dissipation (k-ε) model, using periodic boundaries to satisfy the boundary conditions. A periodic boundary is defined as a boundary where the inlet and outlet velocity distributions are forced to be equal. The magnitude of the velocity, pressure drop and y^+ values were calculated and the mesh was adapted using the maximum y^+ value (for more information refer to Appendix C).

The K-ε turbulence model neglects molecular viscosity and sublayer damping effects, and can only be used in the outer and overlap layers where the log-law

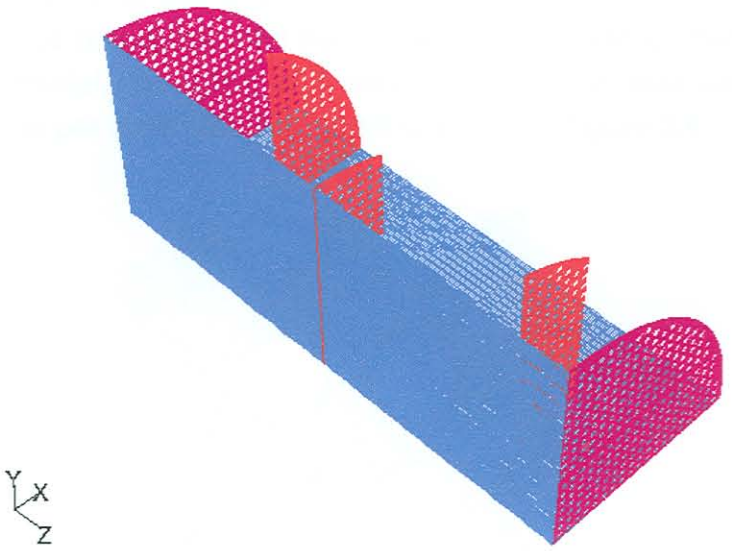

Figure 3.1: Schematic representation of the middle section of the heat exchanger (purple - periodic boundaries, red – baffles and blue – symmetry planes)

holds. The y^+ values on the wall therefore need to be between 35 and 350 according to White (1991) and between 50 and 500 according to FLUENT. The maximum y^+ value for the mesh that was used (1 193 906 cells) was 1 882, which is outside the acceptable region. However, very few cells exceeded a y^+ value of 500 and they were localised at the baffles.

3.2.1 Inertial resistance

To obtain the inertial resistance of the section in the z-direction (refer to figure 3.1 for axes) the pressure drop per meter was calculated at different mass flow rates, as indicated in figure 3.2.

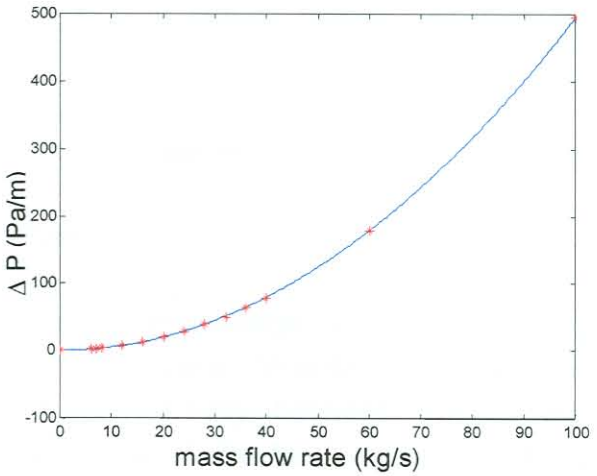

Figure 3.2: Pressure drop per meter through the section in the z-direction

The inertial resistance in the x- and y-directions also needed to be calculated, because the porous part of the inlet section was solved without baffles. For this a more simplified model, consisting of 4 tubes in cross-flow, was used (figure 3.3). The pressure drop per meter for this model is shown in figure 3.4.

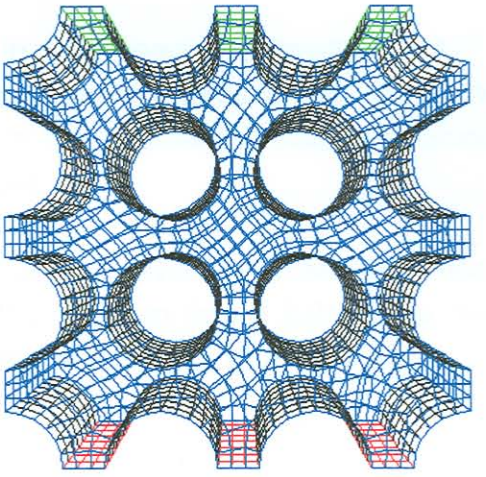

Figure 3.3: FLUENT model of tubes in cross-flow

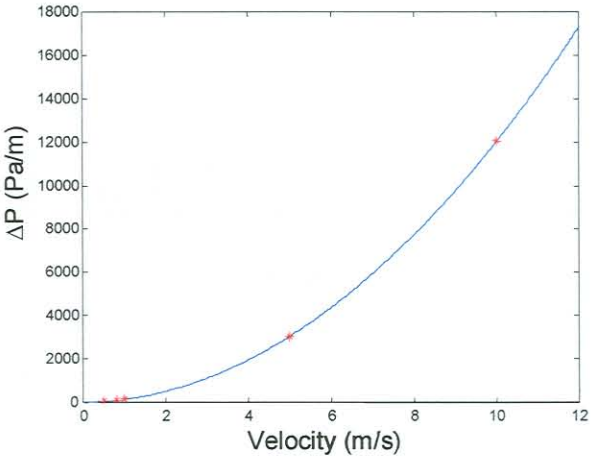

Figure 3.4: Pressure drop per meter in the x and y-direction.

3.2.2 Cross-flow velocities

The HTRI analysis used an average cross-flow velocity value in almost all the excitation frequency calculations. In order to compare the CFD and HTRI results, the average cross-flow velocity between baffles was calculated. Varying distances from the centre of the heat exchanger were used to take the flow patterns into account.

The baffles force the flow in the x-direction, causing much larger cross-flow velocity in the x-direction than in the y-direction. Because of this, the surfaces used to calculate the magnitude of velocity, were chosen in the x-direction. The average cross-flow velocities in the x- and y-directions on the surfaces, were calculated and combined to obtain an average cross-flow velocity magnitude.

Because of the offset in tube spacing between the 12th and 13th tube row (see figure 2.2) the average cross-flow velocity was calculated separately for the two parts. This ensured that the approach cross-flow velocities were calculated and not the gap flow velocities.

Figure 3.5 shows the change in average cross-flow velocity magnitude between a type 3 and type 1 baffle (refer to figure 2.2) in the middle section of the heat exchanger for mass flow rates of 6, 8, 12 and 16 kg/s.

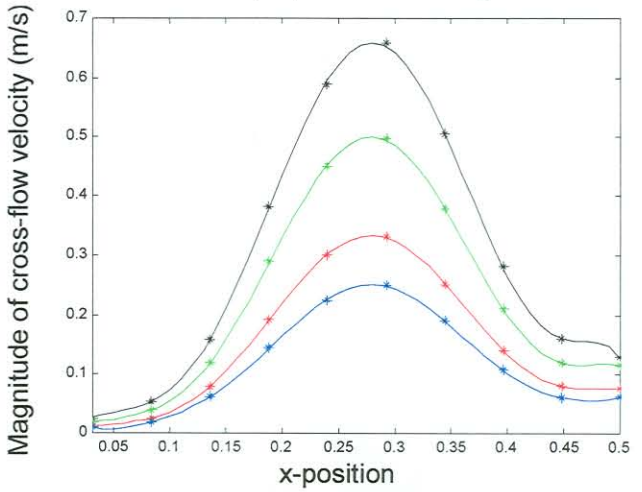

a) bottom section

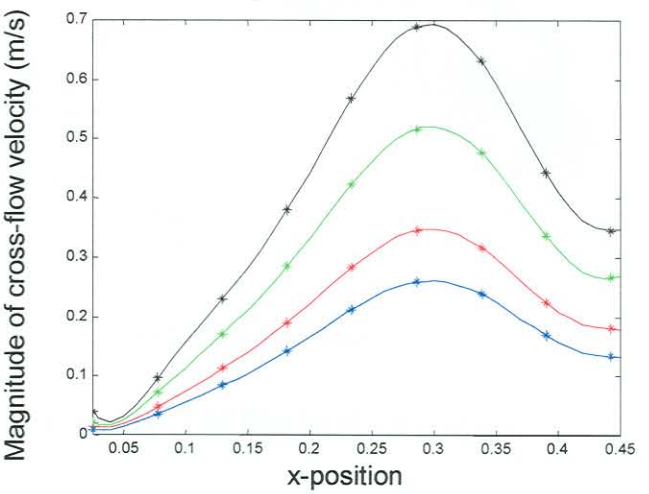

b) top section

Figure 3.5: Velocity magnitude as a function of the x position between baffle type 3 and 1 (blue – 6 kg/s, red – 8kg/s, green – 12kg/s and black – 16 kg/s)

Eighth-order polynomials were fitted through the four sets of data points (figures 3.5 a and b). These polynomials were used to obtain a single equation (for the top and bottom sections respectively) to calculate the magnitude of the cross-flow velocity at any given position (x) and mass flow rate ($\dot{m}$) within the specified range. Only a quarter of the heat exchanger was analysed and the mass flow rate was therefore divided by 4 to obtain the correct velocities through the section.

$$v_{bottom} = 14656.1\frac{\dot{m}}{4}x^8 - 33836.3\frac{\dot{m}}{4}x^7 + 30566.5\frac{\dot{m}}{4}x^6 - 13615.9\frac{\dot{m}}{4}x^5 + 3105.82\frac{\dot{m}}{4}x^4 - 354.814\frac{\dot{m}}{4}x^3 + 22.3272\frac{\dot{m}}{4}x^2 - 0.654188\frac{\dot{m}}{4}x^1 + 0.0132422 \quad 3.1$$

$$v_{top} = -5517.75\frac{\dot{m}}{4}x^8 + 697.8\frac{\dot{m}}{4}x^7 + 8938.07\frac{\dot{m}}{4}x^6 - 8303.33\frac{\dot{m}}{4}x^5 + 3173.48\frac{\dot{m}}{4}x^4 - 615.0\frac{\dot{m}}{4}x^3 + 63.3456\frac{\dot{m}}{4}x^2 - 2.6675\frac{\dot{m}}{4}x^1 + 0.042957 \quad 3.2$$

The same procedure was followed to obtain equations for the cross-flow velocities between baffles type 1 and type 2 and baffles type 2 and type 3 (Appendix C). In figure 3.6 the flow patterns through a section of the heat exchangers are shown with maximum velocity magnitudes (indicated with red) at the baffle plates.

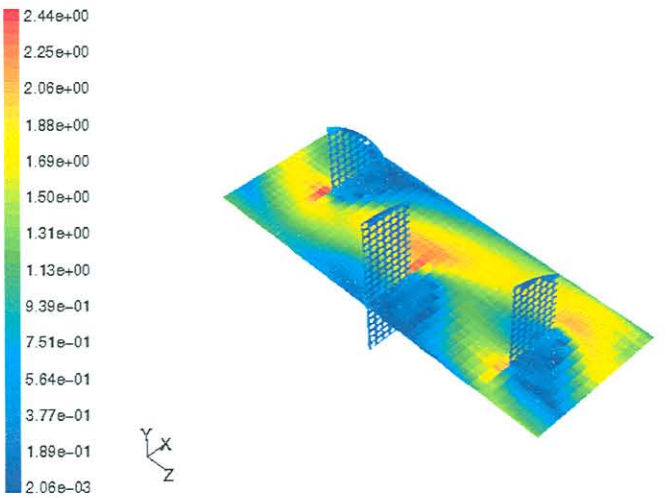

Figure 3.6: Velocity magnitude contour plot through a section of the heat exchanger

3.3 CFD analyses: Inlet section of the heat exchanger

The flow through the inlet section of the heat exchanger was simulated using the porous medium obtained from the previous section, to represent the remaining part of the heat exchanger at the outlet boundary of the inlet section (figure 3.7).

Figure 3.7: Schematic representation of the inlet section

This was done to ensure the necessary back pressure and flow pattern at the outlet boundary.

The adapted mesh consisted of approximately 1.4 million cells. The pressure drop per meter for a mass flow rate of 8 kg/s, was calculated and compared to the value obtained in the previous section and the inertial resistance was adjusted accordingly. This was necessary because the porous section was solved without baffles and the flow could therefore not be forced into the x- or y-directions. The model was then solved for a range of mass flow rates (with a fixed inertial resistance) and the results were again compared with the results of the previous section, as shown in figure 3.8.

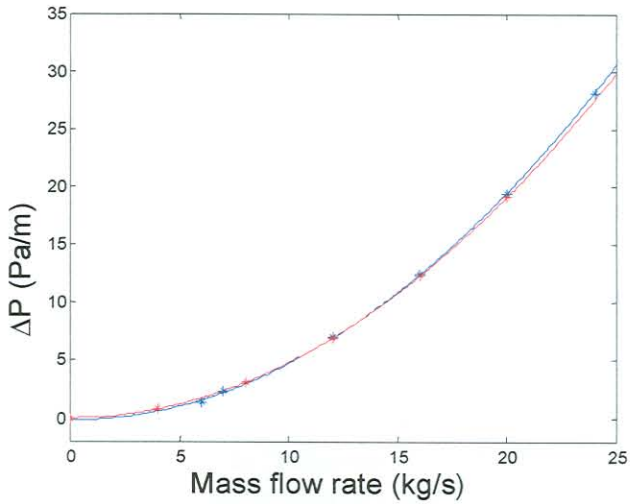

Figure 3.8: Pressure drop per meter
(blue – CFD analyses of repeating section, red – Equivalent porous model)

3.3.1 Cross-flow velocities

For the inlet section, the flow in the y-direction between the tubesheet and the first baffle, as well as the first and second baffle, will be larger, because of the orientation of the inlet. For this reason the surfaces that were used to calculate the average cross-flow velocities in both the x- and y-direction, were chosen in the y-direction. The surfaces between the second and third baffles are the same as for the middle section (see section 3.2.2). Figures 3.9 a) and b) show the average cross-flow velocities between baffle types 1 and 2, as well as between the tubesheet and baffle type 1.

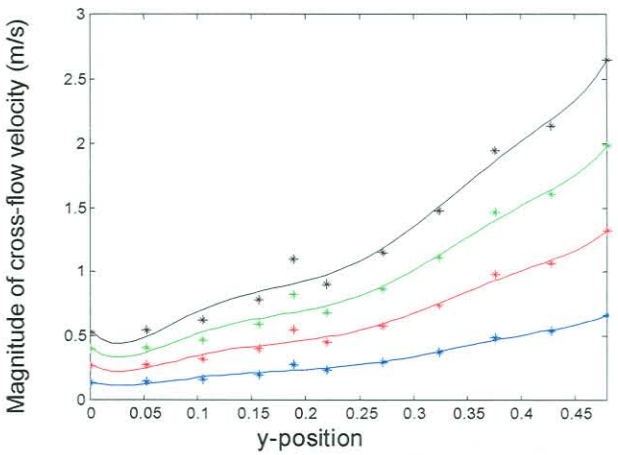

a) Baffles 1 and 2

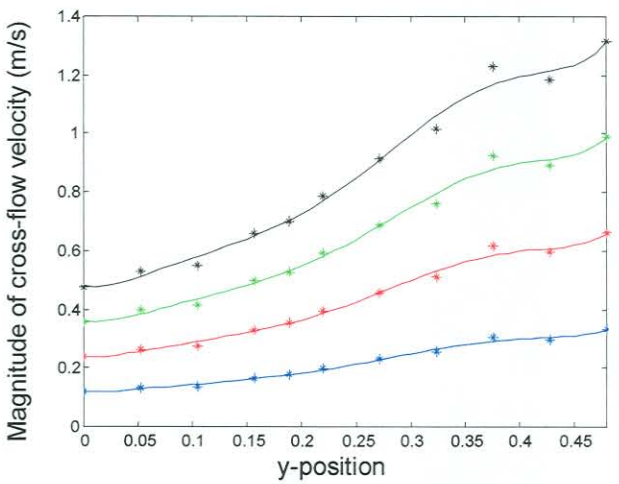

b) Tubesheet and baffle 1

Figure 3.9: Magnitude of average cross-flow velocity (blue-4 kg/s, red – 8 kg/s, green – 12 kg/s and black 16 kg/s)

Sixth-order polynomials were fitted through the data points in figures 3.9 a) and b). In figure 3.9 a) the magnitude of the cross-flow velocities between y-positions 0.15 and 0.2 is higher than the polynomial values due to the larger tube spacing between 12th and 13th tube row. Figure 3.9 b) shows the larger magnitude of

cross-flow velocity at the second tube row (between y-positions 0.35 and 0.4). These polynomials were again used to obtain a single equation to calculate the magnitude of the cross-flow velocity at any given position and mass flow rate within the specified range. Only half of the inlet section was simulated and the mass flow rate was therefore divided by 2, to obtain the correct velocity at the inlet of the heat exchanger.

$$v_{tsbl1} = 333.082\frac{\dot{m}}{2}y^6 - 441.899\frac{\dot{m}}{2}y^5 + 212.266\frac{\dot{m}}{2}y^4 - 45.5719\frac{\dot{m}}{2}y^3 + 4.7624\frac{\dot{m}}{2}y^2 - 0.072717\frac{\dot{m}}{2}y^1 + 0.059951 \quad 3.3$$

$$v_{bl12} = 1034.07\frac{\dot{m}}{2}y^6 - 1548.67\frac{\dot{m}}{2}y^5 + 875.218\frac{\dot{m}}{2}y^4 - 229.245\frac{\dot{m}}{2}y^3 + 28.1241\frac{\dot{m}}{2}y^2 - 1.06629\frac{\dot{m}}{2}y^1 + 0.067350 \quad 3.4$$

Figure 3.10 shows the velocity distribution through the inlet section of the heat exchanger. A small part of the porous section is included in figure 3.10.

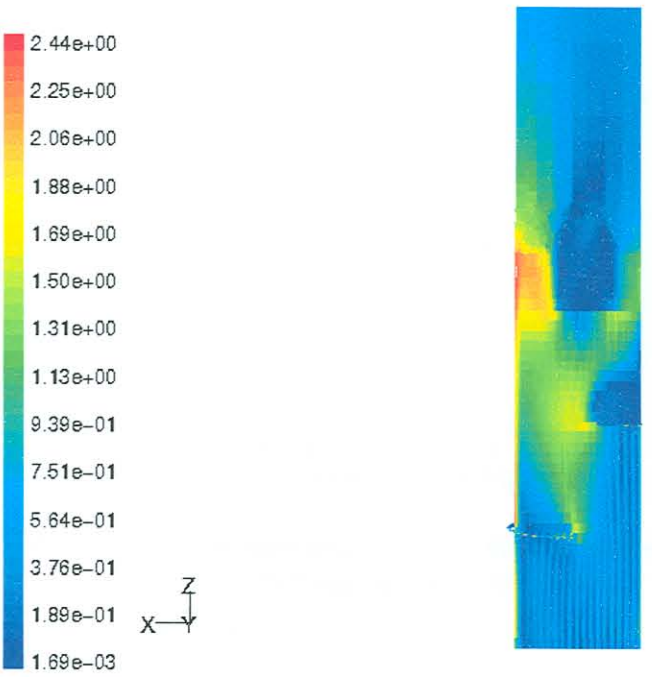

Figure 3.10: Magnitude of velocity over a section of the heat exchanger ($m.s^{-1}$)

3.4 Conclusion

In this chapter, detailed CDF analyses of the heat exchanger were performed to determine the pressure drop, flow patterns and average cross-flow velocities. The average cross-flow velocity values were used to obtain equations that can be used to calculate the magnitude of the cross-flow velocity at any given mass flow rate and position within the specified range. This reduced the computational time to only two simulations, one at the lowest and one at the highest mass flow rate of the range. In figure 3.11, the CFD pressure drop values are compared to the HTRI calculated values. At lower mass flow rates, the pressure drop values for the two methods are the same, but at higher mass flow rates, the CFD pressure drop value is slightly higher than the HTRI value. This is due to the limit in cells used for the analyses as desired in Section 3.2 and Appendix C. Using these pressure drop values to obtain the correct back pressure for the inlet section where the flow velocities are the highest, can further reduce the computational time. The middle-section of the heat exchanger with periodic boundaries need therefore only be analysed at the lowest and highest mass flow rates of the specified range.

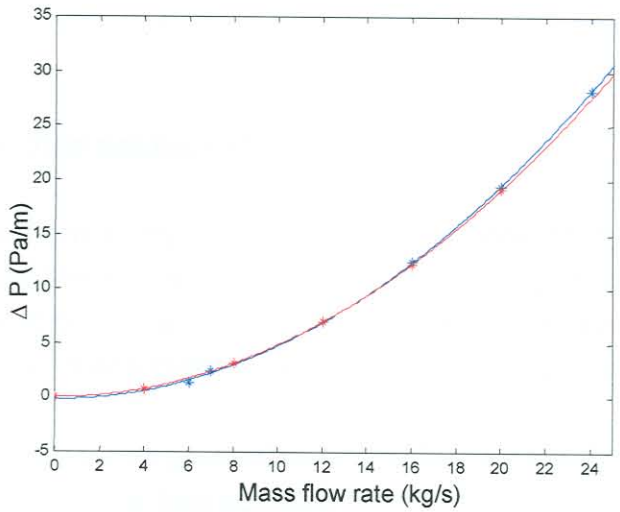

Figure 3.11: Pressure drop per meter through heat exchanger (blue – CFD results, red – HTRI results)